Design and Characterization of a Soft Multi-Axis Force Sensor Using Embedded Microfluidic Channels

Daniel M. Vogt, *Member, IEEE*, Yong-Lae Park, *Member, IEEE*, and Robert J. Wood, *Member, IEEE*

***Abstract*— Thin, highly compliant sensing skins could provide valuable information for a host of grasping and locomotion tasks with minimal impact on the host system. We describe the design, fabrication, and characterization of a novel soft multi-axis force sensor made of highly deformable materials. The sensor is capable of measuring normal and in-plane shear forces. This soft sensor is composed of an elastomer (modulus: 69 kPa) with embedded microchannels filled with a conductive liquid. Depending on the magnitude and the direction of an applied force, all or part of the microchannels will be compressed, changing their electrical resistance. The two designs presented in this paper differ in their flexibility and channel configurations. The channel dimensions are approximately 200 × 200 μm and 300 × 700 μm for the two prototypes, respectively. The overall size of each sensor is 50 × 60 × 7 mm. The first prototype demonstrated force sensitivities along the two principal in-plane axes of 37.0 and −28.6 mV/N. The second prototype demonstrated the capability to detecting and differentiating normal and in-plane forces. In addition, this paper presents the results of a parameter study for different design configurations.**

***Index Terms*— Soft sensors, force sensors, tactile sensors, liquid metal, eutectic gallium indium (eGaIn).**

I. Introduction

THE DEVELOPMENT of soft sensors is a key challenge for wearable electronics [1], soft robots [2]–[4], humanoid robots [5], medical robots [6], [7], dexterous robot manipulators [8], [9], haptic interfaces [10] and countless other applications that require sensors that do not impede the motion of the host. In addition to being soft (modulus $<$1MPa), such sensors must be durable, impact resistant, remain electronically functional when stretched and composed of relatively low-cost raw materials [11]. If these goals are achieved, soft sensors could be worn by humans or existing robot platforms, making devices and robots more human-friendly and human-safe while also expanding the application areas of soft robots.

Manuscript received April 1, 2013; revised June 17, 2013; accepted June 19, 2013. Date of publication July 4, 2013; date of current version September 4, 2013. This work was supported by the Wyss Institute for Biologically Inspired Engineering at Harvard University. D. Vogt and Y.-L. Park contributed equally to this work. The associate editor coordinating the review of this paper and approving it for publication was Prof. Zeynep Celik-Butler.

The authors are with the School of Engineering and Applied Sciences, Harvard University, Cambridge, MA 02138 USA, and also with the Wyss Institute for Biologically Inspired Engineering, Harvard University, Boston, MA 02155 USA (e-mail: dvogt@seas.harvard.edu; ylpark@wyss.harvard.edu; rjwood@eecs.harvard.edu).

Color versions of one or more of the figures in this paper are available online at http://ieeexplore.ieee.org.

Digital Object Identifier 10.1109/JSEN.2013.2272320

One example of such soft sensors is an artificial skin made of an elastomer with embedded microchannels filled with a conductive liquid [12]. When pressure is applied, the cross-sectional areas of the microchannels are reduced, increasing their electrical resistance. When the skin is stretched, the electrical resistance also increases due to the increased channel length and decreased cross-sectional area. Using these principles, properties such as multi-axial strain [12], normal surface pressure [13], [14], and bending curvature [15], [16] can be measured using only soft or liquid-phase materials. However, these sensors are not capable of detecting in-plane (i.e. shear) forces applied to the surface of the sensor. Shear is particularly important for locomotion (e.g. traction) and manipulation (e.g. sensing grasp failure) and also for wearable devices where the loads applied to human skin are critical for comfort. In this work, the same principle of liquid embedded elastomers is employed to extend the capability of soft sensors to detect in-plane forces.

Rigid and flexible microelectromechanical systems (MEMS) based force and shear sensors [17], [18] have been previously reported for applications such as fluid flow measurement [19] and above-knee prosthesis [20]. Various polymer-based flexible tactile sensors that can detect normal and shear forces simultaneously have also been proposed using different approaches. Jiang et al. have developed a shear stress sensing array by forming silicon islands using a reactive-ion etching (RIE) technique [18]. Hwang et al. and Kwon et al. have employed a protruded force element on a strain gauge patterned flexible membrane [21], [22]. Chuang et al. have designed a rigid force element on a polyvinylidene fluoride (PVDF) film encapsulated by a polydimethylsiloxane (PDMS) layer [23]. Instead of strain gauges or piezoresistive elements, Lee et al. have embedded multiple capacitors in PDMS to detect shear forces [24]. Optical sensing is another method to detect small forces accurately, such as optoelectronic components embedded within shear sensors [25]. However, these sensors are not highly deformable due to their rigid electrodes and wire connections.

In this paper, we extend the sensor presented in [26] with a second prototype, study the effect of temperature variation and stretching sensitivity, and examine some design variables that define the soft sensor. This sensor leverages the novelty of using and liquid-phase materials as shown in [12], [13], [15], [16] to measure multi-axis forces, while remaining flexible and stretchable. The sensor is composed of three main compo-

1530-437X © 2013 IEEE

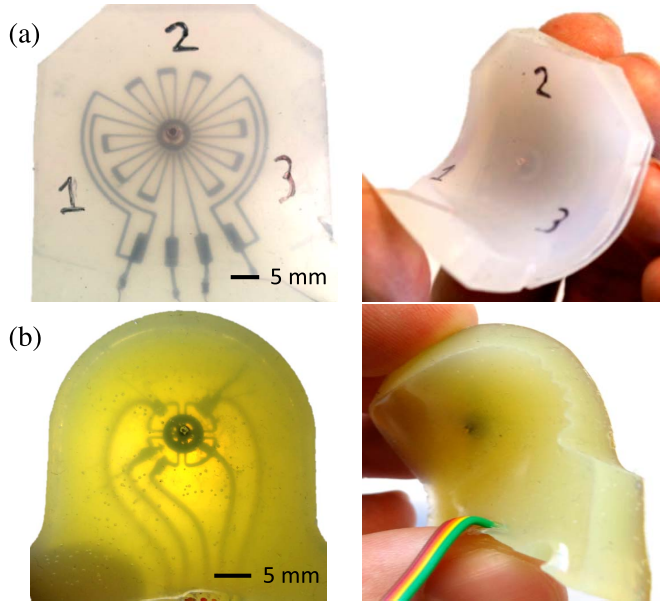

Fig. 1. Soft multi-axis force sensors showing their form factors and deformability. (a) Prototype I with a completely soft base structure. The sensor is both stretchable and flexible. (b) Prototype II with a flex-circuit backing. The sensor is not stretchable but flexible.

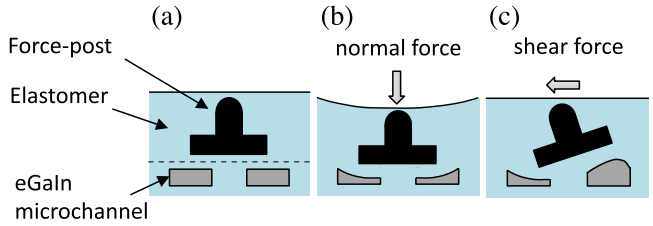

Fig. 2. (a) Description of the different layers of the sensor. (b) Deformation due to a pressure. (c) Deformation due to an in-plane force at the senor surface.

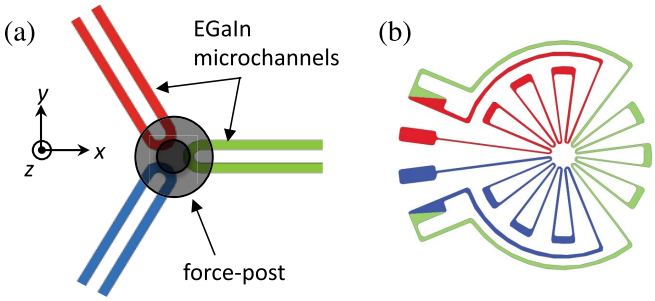

Fig. 3. Microchannel configurations. (a) Three U-shaped microchannels with 120° intervals detect forces in three directions. (b) Three microchannels with increased spatial resolution (current design for Prototype I).

nents: a highly deformable base elastomer material, conductive microfluidic channels, and a force transmission element.

The paper is organized as follows. Sections II and III describe the design, fabrication, and characterization of two soft sensor prototypes. Sections IV and V discuss experimental results from parameter studies and external variable changes, respectively. We conclude with a discussion of future work.

Beyond proprioception for robotic manipulation and locomotion, there are a host of other potential applications for soft shear sensors including smart tires for preventing slippage and new human-machine interfaces.

II. Prototype I

A. Design

The first sensor prototype, shown in Fig. 1, was developed to measure three forces (one normal and two in-plane forces) applied to its top surface. This sensor contains embedded microchannels filled with a liquid metal[1] and a rigid plastic force-post. The force-post is prototyped using a 3D printer[2] before being embedded in a silicone rubber substrate[3] (modulus: 69 kPa, Shore hardness: 00-30).

The sensor is composed of two elastomer layers, as shown in Fig. 2(a). The top layer contains the force-post and the bottom layer contains the eGaIn microchannels (200 μm $\times$ 200 μm, rectangular cross-section) patterned with rotational symmetry, as shown in in Fig. 3. Since we desire three-axis force sensing, we need a minimum of three sensing elements. By arranging three sensing elements in a star pattern, we can decipher in-plane forces in two axes and a normal force. The three channels are separated by 120° and intersect under the force-post. For the sake of wiring, the channels extend out to the perimeter of the sensor. Although the minimum number of sensing elements is three, the addition of more channels can increase the sensor accuracy at the expense of spatial complexity.

Fig. 3(a) shows a simplified representation of the star-shaped microchannel pattern along with the final configuration. The design is compatible with our fabrication process where eGaIn is injected into the channels; the geometry in Fig. 3(b) combines the three sensing elements into one channel, thus facilitating filling.

In addition, although our channel design, shown in Fig. 3(b), is electrically equivalent to the simplified configuration in Fig. 3(a), the microchannles in our design pass underneath the force-post several times, thereby increasing the overall sensitivity. The microchannels can be divided into three major channels, with each channel having eight sub channels, for a total of 24 channels under the force-post.

When a normal force is applied on the surface, the force-post uniformly compresses all channels, resulting in increased electrical resistance in the three channels, as shown in Fig. 2(b). With an in-plane force, the force-post will rotate and press only one or two of the three microchannels depending on the configuration of the channels, which also causes increased resistance of the deformed channels, as shown in Fig. 2(c). By monitoring the resistance changes of the three sensor signals, we can determine the direction and magnitude of the force.

B. Fabrication

The fabrication steps for the sensor prototype are represented in Fig. 4. First, the microchannels are created by

[1]Eutectic Gallium Indium (eGaIn), Sigma-Aldrich, St. Louis, MO, USA.
[2]Connex 500, Objet Geometries, Billerica, MA 01821, USA.
[3]EcoFlex0030, Smooth-On Inc., Easton, PA 18042, USA.

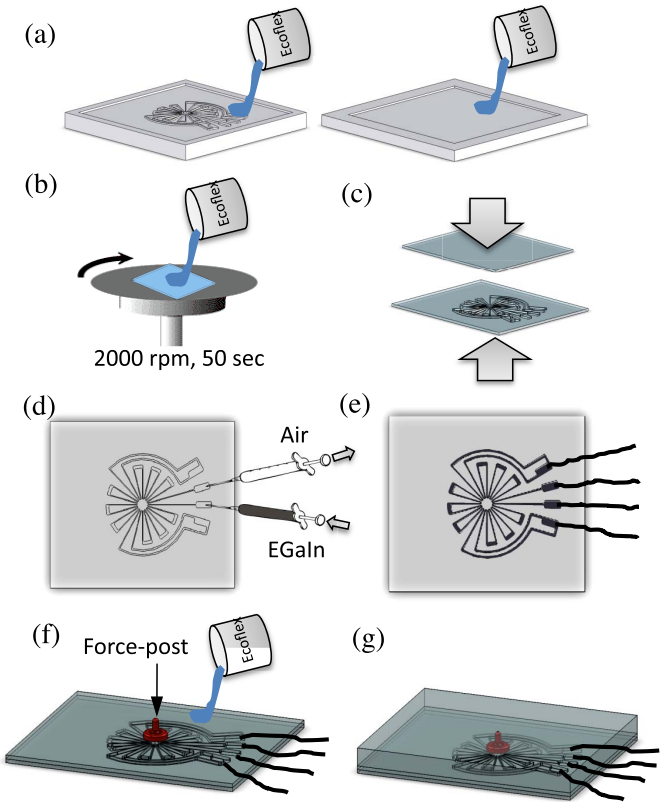

Fig. 4. Fabrication process. (a) Pour liquid elastomer in the molds. (b) Spin coat a thin layer of EcoFlex on the flat surface. (c) Bond the two layers. (d) Inject eGaIn using two syringes. (e) Insert wires. (f) Place the force-post and pour EcoFlex. (g) Finished multi-axis force sensor.

pouring liquid elastomer in two 3D printed molds, shown in Fig. 4(a): one for casting a microchannel patterned top layer and the other for a flat bottom layer. Once cured, these two layers are bonded together by spin coating a thin layer of uncured elastomer, as shown in Fig. 4(b) and (c). The microchannels are then filled with eGaIn in the two middle reservoirs using two syringes (Fig. 4(d)). While one of the syringes injects eGaIn, the other evacuates the air captured in the channel during layer bonding process. Electrical connections are then made using thin wires inserted in each reservoir following the same path as the needle holes. This ensures that the wires are well anchored in the soft sensor (Fig. 4(e)). The force-post is then placed (Fig. 4(f)) and Ecoflex is cast as an upper layer until the force-post is completely covered (Fig. 4(g)). The actual mold used for fabrication and the complete elstomer layer with an embedded eGaIn microchannel are shown in Fig. 5.

C. Experimental Setup

By applying a constant current source in series with all three channels, changes in resistance from applied pressures can be read as voltage changes. In order to characterize the sensitivity of the sensors, we describe the experimental setup that enables us to apply a known load and read the resulting voltage change.

1) Test Bench Integrated With a Multi-Axis Force Sensor: To characterize the sensor, we first need to apply a known

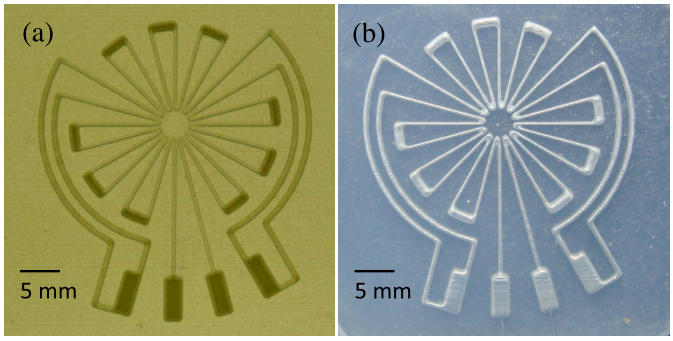

Fig. 5. (a) Photo of the 3D printed mold used for fabricating the microchannel elastomer structure. (b) Photo of the microchannel embedded elastomer sheet after injecting eGaIn.

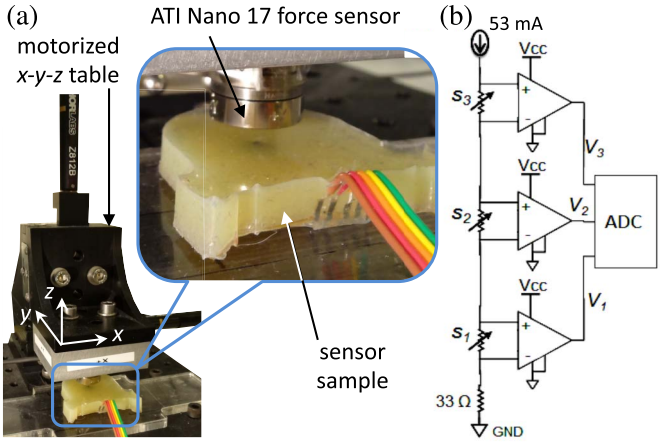

Fig. 6. (a) Translation stage mounted with a force sensor. (b) Schematic of the electronic circuit with S1, S2, and S3 corresponding to the variable resistances of the soft multi-axis force sensor.

load. This can be achieved by mounting a 6-axis force and torque sensor to a 3-axis translation stage. Fig. 6(a) shows the motorized translation stage[4] chosen for this purpose. This translation stage has a travel range of 13 mm and a load capacity of 44.1 N.

A custom-made interface connects the commercial multi-axis force sensor[5] to the 3-axis translation stage. The force sensor is then connected to a USB data acquisition card[6] on a PC, and the data can be processed in Matlab®.

2) Signal Conditioning Circuit: In order to evaluate the force response, a signal conditioning circuit, shown in Fig. 6(b), was prepared. The circuit provides constant current through the three sensing elements that are electrically equivalent to three variable resistances connected in series. In this circuit, the voltage change across each sensing element is amplified (46×) using an operational amplifier. The amplified voltages are then read by a USB data acquisition tool.

D. Sensor Characterization

To characterize the soft sensor, forces are applied in the x, y, and z directions, as defined in Fig. 6, using the translation

[4]MT3/M-Z8, Thorlab, Newton, New Jersey, USA.
[5]F/T Nano 17, ATI Industrial Automation, Apex, NC 27539 USA.
[6]NI USB-6210, National Instruments, Austin, TX 78759, USA.

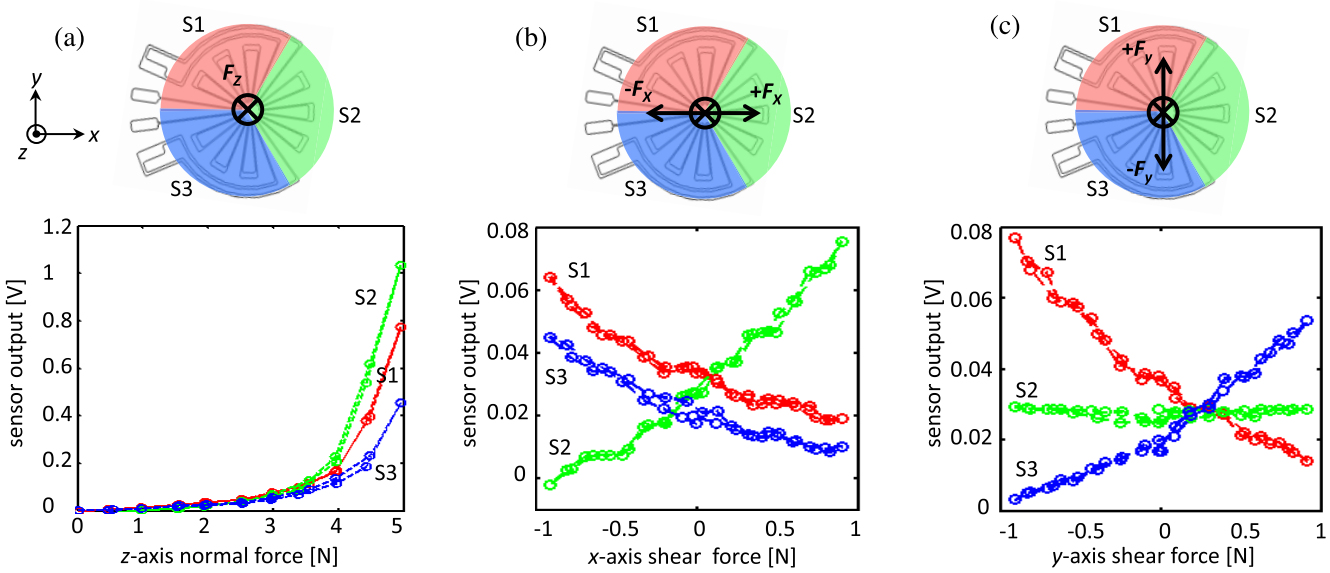

Fig. 7. Force characterization results of Prototype I. (a) z-axis normal force response. (b) x-axis shear force responses. (c) y-axis shear force response.

stage. The commercial multi-axis force sensor measures the applied forces and the sensor signal was measured as described in Section II-C.1. During the tests, the force sensor was in direct contact with the top surface of the soft sensor. To prevent the two surfaces from slipping while applying in-plane forces, a thin layer of sandpaper was firmly attached to the surface of the commercial sensor.

A Matlab® graphical user interface (GUI) was prepared to easily record the reference force values and the sensor signals. This GUI allowed us to see real-time force responses. In our experiments, the sensor signal was sampled at 100 Hz, and each recorded data point was the average of the most recent 50 samples. Two tests were conducted for normal force response in the z-axis and lateral force responses in x- and y-axes, respectively. Note that this is only a static characterization of the sensor.

To estimate the normal or the shear forces from the sensor's resistance change, the method in [12] can be used by approximating the sensor response as linear and generating a 3×3 calibration matrix using the least mean square method.

1) Normal Force Response: When applying a normal force, the force-post compresses all three microchannels evenly, and the resistances of the three microchannels exponentially increased, as discussed in [13]. In this experiment, we gradually increased the force in the z-axis from 0 N to 6 N, and then gradually released the force back to zero to evaluate hysteresis. The result of this experiment is shown in Fig. 7(a).

2) In-Plane Force Response: To measure in-plane forces, a pre-load normal to the sensor's surface is required in order to avoid slippage between the two surfaces. An initial vertical force of 2 N was applied and regulated throughout the experiment. We then translated the force sensor along either the x- or y- axes and measured the applied force and sensor signal changes. Fig. 7(b) and (c) show the test results. The sensor prototype was loaded in the positive direction first starting from zero, unloaded back to zero, loaded in the negative direction passing the zero point and finally unloaded back to zero again, making a complete loop. The results displays more linear response to in-plain forces relative to normal forces. There was negligible hysteresis in any of trials.

3) Failure Test With Large Strain: In addition to force characterization, a strain test was conducted to check the failure point of the sensor. When the sensor is stretched, the microchannels elongates and their cross-sections are decreased, resulting in increased electrical resistance. However, the sensor still remains functional until one of the microchannels is broken or the electrode looses contact. To check the maximum strain the sensor can tolerate while the sensor was still functional, a strain test was conducted using a commercial materials tester[7], as shown in Fig. 8(a), and the resistance change of one of the three microchannels was recorded. The sensor was able to tolerate up to approximately 180% strain, as shown in Fig. 8(b).

E. Results and Discussion

The experiments described in Sections II-D.1 and II-D.2 fully characterize the static force response of the sensor. As shown in Fig. 7, there is little hysteresis in the sensor signals. This small hysteresis may be due to the constraints applied by our experimental setup. The experiments described in Section II-D are based on position change of the commercial force sensor in contact with the soft force sensor. Therefore, it is not surprising that we do not see significant hysteresis in the sensor signals. If the surface of the sensor was free, we would expect to see some hysteresis due to the viscoelastic nature of the elastomer materials. However, given the scope of applications we envision - where objects are in constant direct contact with the sensor - we believe that the characterization in Section II-D is most appropriate.

[7]Instron 5544A, Instron, Norwood, MA 02062, USA.

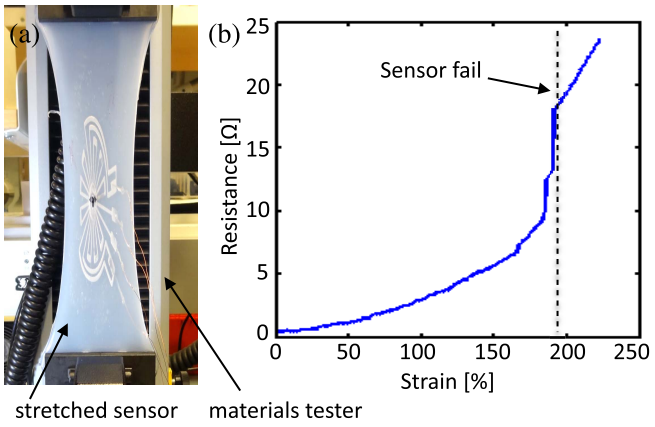

Fig. 8. (a) Strain test setup. (b) Channel resistance as the sensor is strained to failure.

As shown in Fig. 7(a), the normal force response is nonlinear. This is expected due to the nonlinear reduction rate of the cross-sectional area of the microchannel [13]. This nonlinearity can be alleviated by changing the cross-sectional geometry of the microchannel as shown in [14]. It is important to also notice that the three sensor responses are not exactly the same. This may be due to slight differences in the channel geometries and in the wire connections. In addition, the current design makes the length of the S2 channel slightly longer than the other two, resulting in a higher nominal resistance.

As can be seen in Fig. 7(b) and (c), the in-plane responses show strong directional sensitivity. For example, positive force along the x-axis is detected by an increase in S2 and a simultaneous decrease in S1 and S3. The offset between S1 and S3 is likely due to the difference in the response to the initial pressure. When applying force along the y-axis, S1 and S3 change symmetrically as expected. S2 stays at its initial level as the applied force is perpendicular to its sensitivity axis.

Using a linear fit, we can estimate the in-plane force sensitivity of 37.0 mV/N for the x-axis and -28.6 mV/N for the y-axis (with S1). Due to its nonlinear response, the sensitivity to normal force, when measured with S2, varies from approximately 27.8 mV/N for forces bellow 3.4 N and 572.7 mV/N for pressures over 4.1 N.

The strain to failure test (Fig. 8) shows how the resistance of the microchannel changes with increased strain. The resistance consistently increased with strain increase. However, there was an abrupt resistant increase at 180% strain, which indicated failure of the sensor. Although the sensor remains electrically conductive beyond 180% strain, it is no longer functional as designed.

III. Prototype II

Some applications require mechanical flexibility of the sensor but not necessarily stretchability, e.g. when fixed on a flat contact surface of a gripper. In this case, the sensor design can be modified to be more robust by replacing eGaIn microchannel wiring with a copper flex-circuit, as shown in Fig. 9. In this design, eGaIn microchannels are used only as the sensing element and not as wires.

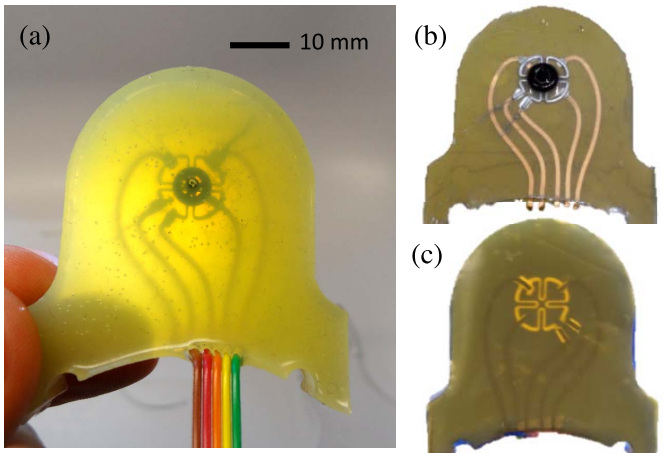

Fig. 9. Photos of Prototype II. (a) Complete prototype showing embedded force post and flex-circuit. (b) Top side of the sensor before adding the elastomer layer. (c) Bottom side of the sensor showing copper traces.

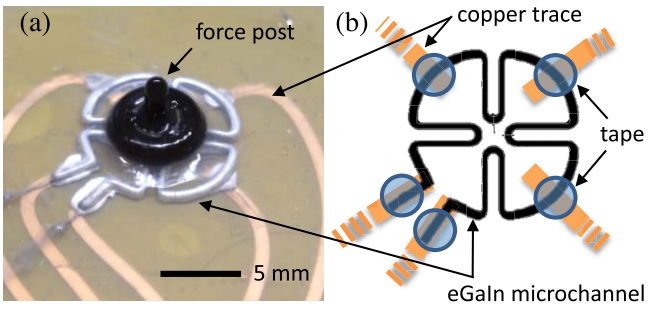

Fig. 10. (a) Detail of the microchannels aligned on copper traces. (b) Four-component microchannel design used for this sensor.

One of the advantages of this design is that the flexible copper wiring reduces the chance of false sensor signals that can be caused by unintended mechanical stimuli to the wiring area. Also, this flex-circuit design allows us to directly embed electronics in the sensor. Since the electrical connections are made between eGaIn microchannels and copper traces on the flex circuit, the length of the microchannels was kept as short as possible.

A. Fabrication

Compared to the fabrication method described in II-B, some modifications were made in order to bond the elastomer layer to the flex circuit. The flex-circuit[8] is prepared using a Kapton® backed copper foil. After spin-coating photoresist[9] on the copper foil, the copper traces are patterned by raster-machining the coated photoresist using a diode-pumped solid state (DPSS) laser and etching with ferric chloride.

Once the copper traces are patterned, tape patches are placed where the electrical conduction between the eGaIn and the copper is necessary (Fig. 10 (b)). This protects the conductive interface areas between eGaIn and copper when a thin layer of silicone adhesive[10] is spin-coated. Due to its high viscosity,

[8]Pyralux 18μm copper, 25μm polyimide (Kapton®).
[9]Shipley SP 24D.
[10]Elastosil RTV Sealant E 951, Wacker Chemical, Adrian, MI 49221, USA.

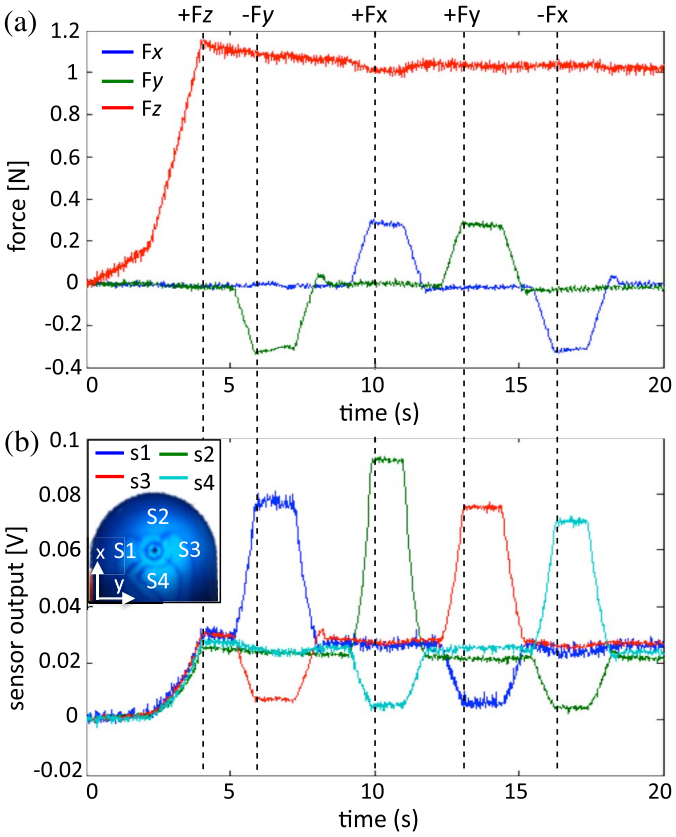

Fig. 11. Characterization results (sampling at 100 Hz). (a) Applied force measured by the commercial multi-axis force sensor. (b) Soft sensor signals.

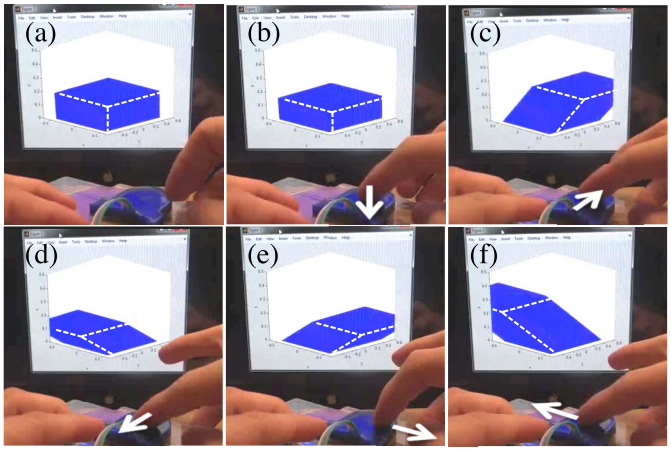

Fig. 12. Snap shots from a real-time visualization system. (a) No stimulus. (b) z-axis normal force. (c) $+x$-axis shear force. (d) $-x$-axis shear force. (e) $+y$-axis shear force. (f) $-y$-axis shear force.

the spin coating speed is higher (3500 rpm, 50 sec.) than in the process described in II-B. The tape patches are then removed, and the elastomer layer with microchannels(300 μm $\times$ 700 μm) is aligned and placed on the flex-circuit. After the adhesive cures, eGaIn is injected in the microchannels, wires are soldered on the copper traces, and the force-post is embedded in the same way as described in II-B.

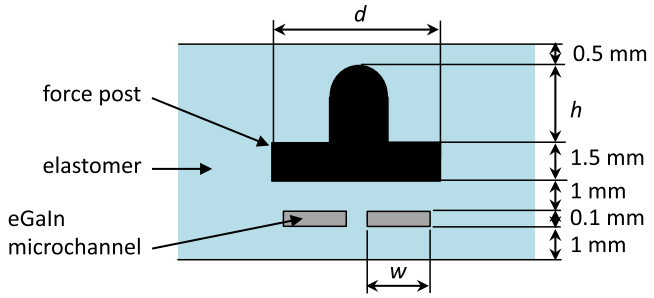

Fig. 13. Primary parameters defining the soft sensors.

B. Characterization and Results

While the previous design has three separate microchannels, the minimum for detecting three forces, this sensor has four microchannels for information redundancy, as shown in Fig. 10. Thus, we have four sensor signals in the experimental result. In this experiment, a normal force of 1.2 N is applied first at a rate of 0.05 mm/s, and then a force of 0.2 N is applied in four in-plane directions ($+x$, $-x$, $+y$, and $-y$) at a rate of 0.3 mm/s.

Fig. 11 shows the experimental result. The four signals from the soft sensor are consistent with those of the commercial force sensor. Fig. 12 shows snap shots of a real-time monitoring system for multi-axis force sensing.

IV. Parameter Study for Sensor Design

In order to better understand the effect of different mechanical parameters on sensor performance, a set of experiments was conducted. Although there may be many parameters that can be controlled, three important parameters related to sensitivity were selected for this study: the width (w) of the microchannels, the diameter (d) and the height (h) of the force-posts (Fig. 13). Other parameters were kept constant. The sensitivity was defined by the slope of the linear approximation of the sensor signal under shear loads.

A. Microchannel Width

To evaluate the effect of microchannel width, a test sample was prepared, as shown in Fig. 14(a), that contains four microchannels with different widths (w = 300, 400, 500, and 600 μm). Four identical force-posts were embedded above the microchannels. The diameter (d) and height (h) of the force-posts were fixed at 6 mm and 3.5 mm, respectively. The sample was tested for unidirectional in-plane force with a pre-loaded normal force.

The experimental results in Fig. 15(a) show that increased channel width yields increased sensitivity. This is due to the reduced aspect ratio of the microchannel which requires less force for the channel to be deformed. However, if the channel width exceeds a certain level, we presume that the sensitivity decreases because the microchannel requires a relatively large pressure area to be compressed while the diameter of the force-post is fixed, which requires more rotation of the force-post.

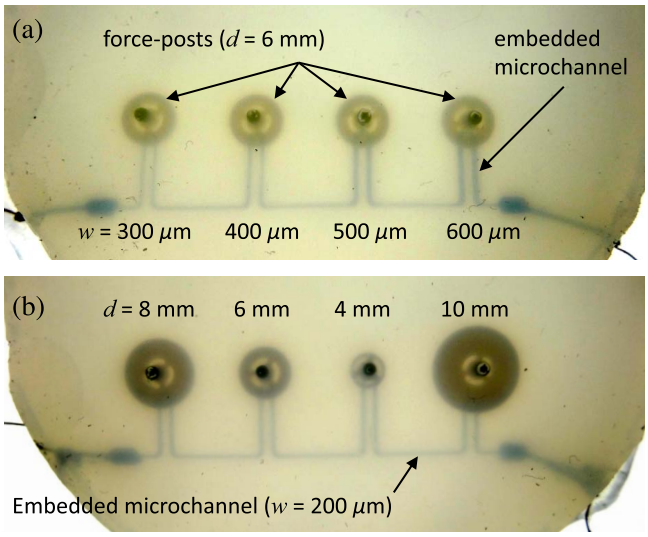

Fig. 14. Parameter study test samples. (a) Multiple microchannel widths. (b) Multiple force-post diameters.

B. Force-Post Diameter

In this experiment, with the microchannel width and force-post height fixed ($w = 200$ μm and $h = 3.5$ mm), four different of the force-post diameters ($\phi = 4$, 6, 8 and 10 mm) were tested, as shown Fig. 14(b).

The experimental result is shown in Fig. 15(b). The result shows that an increase in force-post diameter significantly decreases the sensitivity since an increase in diameter requires larger forces to rotate the force-post. Furthermore, larger force-posts do not engage a larger channel area.

C. Force-Post Height

Four different heights ($h = 0.5$, 1.5, 2.5 and 3.5 mm) of the force post were also tested. In this test, the microchannel width and the force-post diameter were fixed at 500 μm and 6 mm, respectively.

The experimental result is shown in Fig. 15(c). In the high range of height, such as 2.5 mm or 3.5 mm, a higher force-post results in greater sensitivity, since a longer force-post requires less force to create the same moment. However, for lower heights, the sensitivity is greater with lower height. In this case, we suppose that the force-post is squeezed down with shear force rather than being rotated. Thus, the thinner layer above the microchannel with a lower force-post increases sensitivity. However, without allowing a rotational degree of freedom, it is not possible to detect shear forces in different directions as intended.

Fig. 16 compares the results from the parameter study. The sensitivities were determined from the linear fits of the experimental results, and they were compared in the three sets of experiments.

The parameter studies allow us to elucidate sensor design rules as described above. We do not prescribe specific values values for the sensor - these should be tailored to the desired application. However, the parameter studies do hint at optimal configurations warranting more detailed future studies.

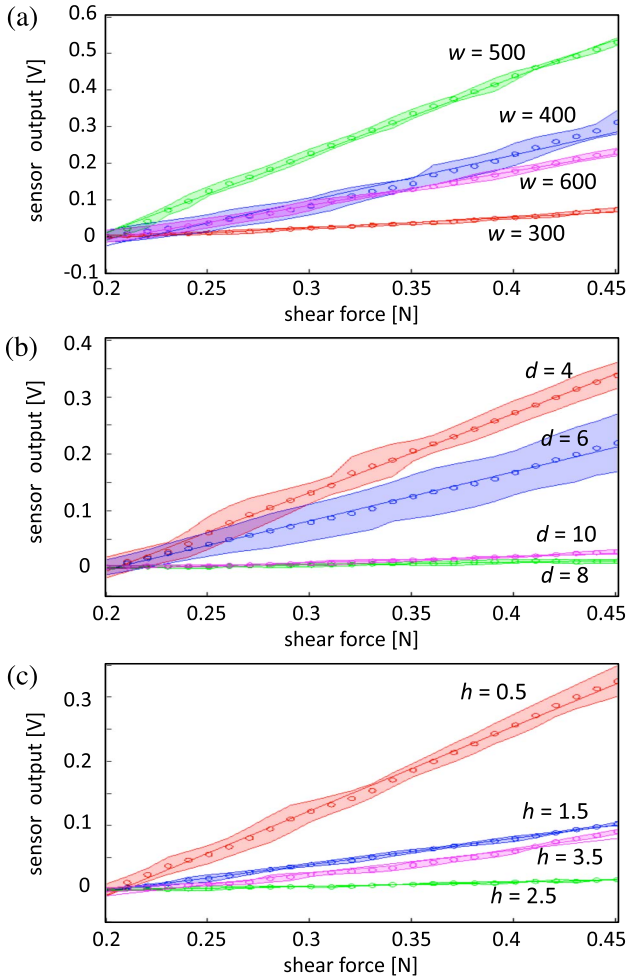

Fig. 15. Parameter study experimental results: (a) channel width, (b) force-post diameter, and (c) force-post height. (circle: mean value of three tests, colored band: standard deviation, solid line: linear fit of all three tests.)

V. External Variable Test

In addition to the design parameters, the sensor prototype was also tested under different external variables. This section provides the experimental results of the sensitivity changes with different temperatures and pre-strains.

A. Temperature Sensitivity

The sensitivity of the sensor in response to temperature variation is important for the envisioned applications. We placed one of the single channel test samples ($d = 6$mm, $h = 3.5$mm and $w = 300\mu$m in Fig. 14(a)) on a hot plate (Fig. 17(a)) and applied a normal force using the same material tester as in II-D.3. The temperature is increased from ambient to 70C and a normal pressure test is done after allowing the temperature to stabilize for a period of ten minutes.

The result (Fig. 17(b)), showed that there is no significant variation in the sensor sensitivity with temperature changes. The changes of the nominal resistance at rest with the three temperatures were also negligible.

B. Pre-strain Sensitivity

The sensor remains electronically functional when stretched, but it is important to understand how the sensitivity is affected

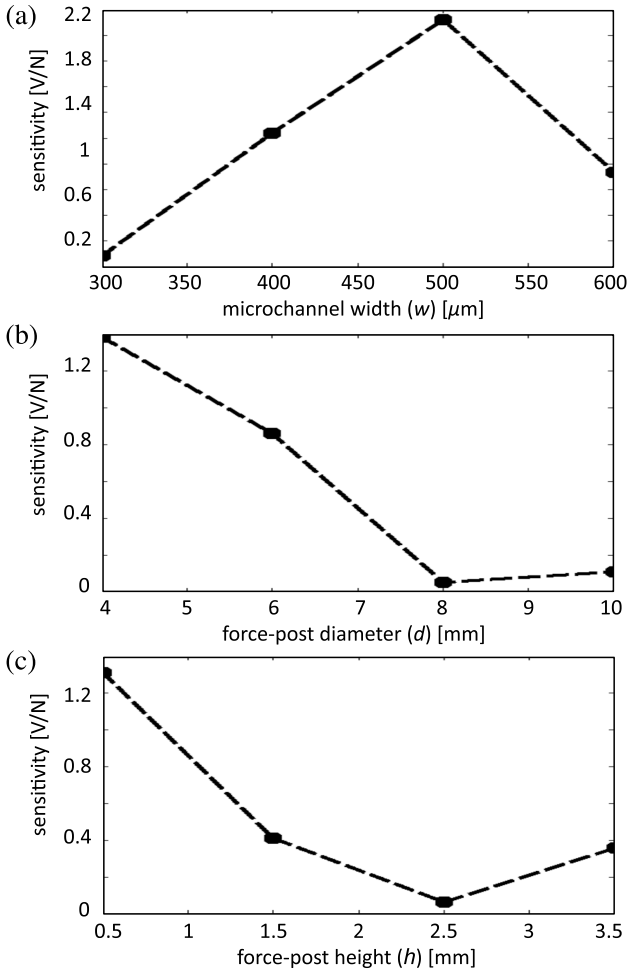

Fig. 16. Sensitivity as a function of (a) channel width, (b) force-post diameter, and (c) force-post height.

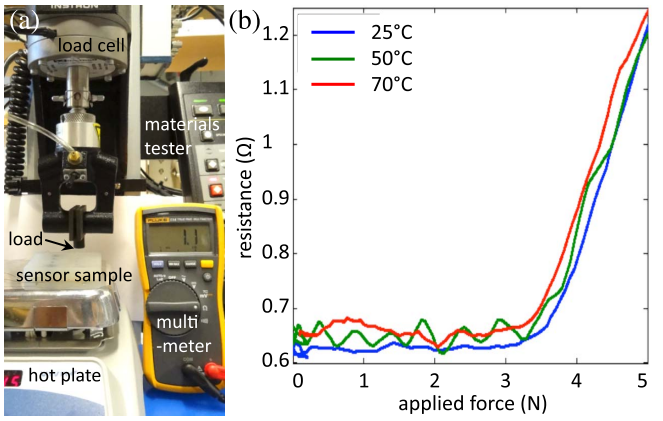

Fig. 17. Temperature test. (a) Experimental setup. (b) Sensor response for different temperatures.

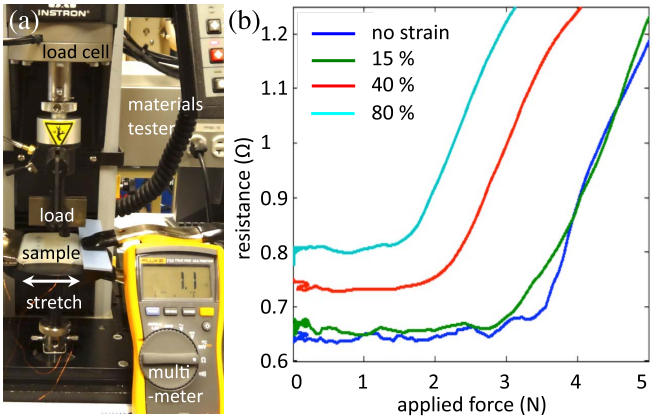

Fig. 18. Strain test. (a) Experimental setup. (b) Sensor response under different pre-strains.

by strain. In order to do so, an experiment has been conducted using a simplified version of the sensor used in Section IV ($d = 6$mm, $h = 3.5$mm and $w = 300\mu$m). This sensor is fixed to the same material tester (Fig. 18(a)) used in Section II-D.3, and a normal pressure test is done while holding the sensor in several configurations (0, 16.7, 41.7 and 83.3 % strain).

The result (Fig. 18(b)) shows increased nominal resistance offset with increased pre-strains. This increase resulted in the decrease of the minimum detectable force. However, there was no significant changes in the sensitivity (slope). Although not shown in this test, pressure responses usually show relatively high hysteresis in addition to nonlinearity, as reported in [12], [14]. However, the hysteresis and nonlinearity could be significantly reduced by changing the cross-sectional geometries of microchannels, as shown in [14], [27].

VI. Conclusion

This study describes the design, fabrication, and characterization of two different prototypes of a novel soft multi-axis force sensor. These sensors can not only detect the normal force applied to the top surface but also measure the direction and magnitude of in-plane (i.e. shear) forces.

Each of these prototypes offers advantages and disadvantages depending on the application they are intended for. While the first prototype is both flexible and stretchable, undesired pressure or strain on eGaIn wiring affects the sensor signals. This potential limitation was solved in the second prototype using an embedded flex-circuit as the substrate.

The modification of some of the parameters has also been studied. It gives a better understanding of the behavior of the sensor and provides a guideline for designing soft sensors for a specific application. Moreover, further miniaturization of the force post and the microchannel dimensions would allow an array of micro channels to localize shear forces along the sensor's surface.

Consider an example application where such sensors are fitted to a robotic hand to test grasping with closed-loop force control. The idea is to lift an object using minimal normal force. We speculate that, with the in-plane force information, the robot will be able to determine the quality of a static grasp and also detect slippage and grasp failure.

References

[1] D. Marculescu, R. Marculescu, N. Zamora, P. Stanley-Marbell, P. Khosla, S. Park, S. Jayaraman, S. Jung, C. Lauterbach, W. Weber, T. Kirstein, D. Cottet, J. Grzyb, G. Troster, M. Jones, T. Martin, and Z. Nakad, "Electronic textiles: A platform for pervasive computing," *Proc. IEEE*, vol. 91, no. 12, pp. 1995–2018, Dec. 2003.

[2] Y.-L. Park, B. Chen, D. Young, L. Stirling, R. J. Wood, E. Goldfield, and R. Nagpal, "Bio-inspired active soft orthotic device for ankle foot pathologies," in *Proc. IEEE/RSJ Int. Conf. Intell. Robots Syst.*, San Francisco, CA, USA, Sep. 2011, pp. 4488–4495.

[3] Y.-L. Park, B. Chen, C. Majidi, and R. J. Wood, "Active modular elastomer sleeve for soft wearable assistance robots," in *Proc. IEEE/RSJ Int. Conf. Intell. Robots Syst.*, Vilamoura, Portugal, Oct. 2012, pp. 1595–1602.
[4] R. F. Shepherd, F. Ilievski, W. Choi, S. A. Morin, A. A. Stokes, A. A. Mazzero, X. Chen, M. Wang, and G. M. Whitesides, "Multigate soft robot," *Proc. Nat. Acad. Sci. USA*, vol. 108, no. 51, pp. 20400–20403, 2011.
[5] R. Tajima, S. Kagami, M. Inaba, and H. Inoue, "Development of soft and distributed tactile sensors and the application to a humanoid robot," *Adv. Robot.*, vol. 16, no. 4, pp. 381–397, 2002.
[6] P. Puangmali, K. Althoefer, L. Seneviratne, D. Murphy, and P. Dasgupta, "State-of-the-art in force and tactile sensing for minimally invasive surgery," *IEEE Sensors J.*, vol. 8, no. 4, pp. 371–381, Apr. 2008.
[7] Y.-L. Park, S. Elayaperumal, B. Daniel, S. C. Ryu, M. Shin, J. Savall, R. J. Black, B. Moslehi, and M. R. Cutkosky, "Real-time estimation of 3-D needle shape and deflection for MRI-guided interventions," *IEEE/ASME Trans. Mech.*, vol. 15, no. 6, pp. 906–915, Dec. 2010.
[8] Y.-L. Park, S. C. Ryu, R. J. Black, K. Chau, B. Moslehi, and M. R. Cutkosky, "Exoskeletal force-sensing end-effectors with embedded optical fiber-bragg-grating sensors," *IEEE Trans. Robot.*, vol. 25, no. 6, pp. 1319–1331, Dec. 2009.
[9] A. M. Dollar and R. D. Howe, "The highly adaptive SDM hand: Design and performance evaluation," *Int. J. Robot. Res.*, vol. 29, no. 5, pp. 585–597, 2010.
[10] A. Okamura and M. Cutkosky, "Feature detection for haptic exploration with robotic fingers," *Int. J. Robot. Res.*, vol. 20, no. 12, pp. 925–938, 2001.
[11] V. J. Lumelsky, M. S. Shur, and S. Wagner, "Sensitive skin," *IEEE Sensors J.*, vol. 1, no. 1, pp. 41–51, Jun. 2001.
[12] Y.-L. Park, B. Chen, and R. J. Wood, "Design and fabrication of soft artificial skin using embedded microchannels and liquid conductors," *IEEE Sensors J.*, vol. 12, no. 8, pp. 2711–2718, Aug. 2012.
[13] Y.-L. Park, C. Majidi, R. Kramer, P. Berard, and R. J. Wood, "Hyperelastic pressure sensing with a liquid-embedded elastomer," *J. Micromech. Microeng.*, vol. 20, no. 12, p. 125029, 2010.
[14] Y.-L. Park, D. Tepayotl-Ramirez, R. J. Wood, and C. Majidi, "Influence of cross-sectional geometry on the sensitivity and hysteresis of liquid-phase electronic pressure sensors," *Appl. Phys. Lett.*, vol. 101, no. 19, pp. 191904-1–191904-4, 2012.
[15] C. Majidi, R. Kramer, and R. Wood, "A non-differential elastomer curvature sensor for softer-than-skin electronics," *Smart Mater. Struct.*, vol. 20, no. 10, p. 105017, 2011.
[16] R. Kramer, C. Majidi, R. Sahai, and R. J. Wood, "Soft curvature sensors for joint angle proprioception," in *Proc. IEEE/RSJ Int. Conf. Intell. Robots Syst.*, San Francisco, CA, USA, Sep. 2011, pp. 1919–1926.
[17] A. Barlian, S. Park, V. Mukundan, and B. Pruitt, "Design and characterization of microfabricated piezoresistive floating element-based shear stress sensors," *Sens. Actuators A, Phys.*, vol. 134, no. 1, pp. 77–87, 2007.
[18] F. Jiang, G.-B. Lee, Y.-C. Tai, and C.-M. Ho, "A flexible micromachine-based shear-stress sensor array and its application to separation-point detection," *Sens. Actuators A, Phys.*, vol. 79, no. 3, pp. 194–203, 2000.
[19] Y. Xu, Y. Tai, A. Huang, and C. Ho, "IC-integrated flexible shear-stress sensor skin," *J. Microelectromech. Syst.*, vol. 12, no. 5, pp. 740–747, 2003.
[20] M. Hsieh, Y. Fang, M. Ju, G. Chen, J. Ho, C. Yang, P. Wu, G. Wu, and T. Chen, "A contact-type piezoresistive micro-shear stress sensor for above-knee prosthesis application," *J. Microelectromech. Syst.*, vol. 10, no. 1, pp. 121–127, 2001.
[21] E.-S. Hwang, J.-H. Seo, and Y.-J. Kim, "A polymer-based flexible tactile sensor for both normal and shear load detections and its application for robotics," *J. Microelectromech. Syst.*, vol. 16, no. 3, pp. 556–563, 2007.
[22] H. Kwon, J. Kim, and W. Choi, "Development of a flexible three-axial tactile sensor array for a robotic finger," *Microsyst. Technol.*, vol. 17, no. 12, pp. 1721–1726, 2011.
[23] C.-H. Chuang, Y.-R. Liou, and C.-W. Chen, "Detection system of cincident slippage and friction coefficient based on a flexible tactile sensor with structural electrodes," *Sens. Actuators A, Phys.*, vol. 188, pp. 48–55, Dec. 2012.
[24] H.-K. Lee, J. Chung, S.-I. Chang, and E. Yoon, "Normal and shear force measurement using a flexible polymer tactile sensor with embedded multiple capacitors normal and shear force measurement using a flexible polymer tactile sensor with embedded multiple capacitors," *J. Microelectromech. Syst.*, vol. 17, no. 4, pp. 934–942, 2008.
[25] J. Missinne, E. Bosman, B. V. Hoe, G. V. Steenberg, S. Kalathimekkad, P. V. Daele, and J. Vanfleteren, "Flexible shear sensor based on embedded optoelectronic components," *IEEE Photon. Technol. Lett.*, vol. 23, no. 12, pp. 771–773, Jun. 2011.
[26] D. Vogt, Y.-L. Park, and R. J. Wood, "A soft multi-axis force sensor," in *Proc. IEEE Sensors Conf.*, Taipei, Taiwan, Oct. 2012, pp. 1–4.
[27] D. Tepayotl-Ramirez, T. Lu, Y.-L. Park, and C. Majidi, "Collapse of triangular channels in a soft elastomer," *Appl. Phys. Lett.*, vol. 102, no. 4, pp. 044102-1–044102-4, 2013.

Daniel M. Vogt received the B.S. degree in computer science from the Engineering School of Geneva, in 2005, and the M.S. degree in microengineering from the Swiss Federal Institute of Technology (EPFL), in 2011 with a minor in Management of Technology and Entrepreneurship. A robotics enthusiast, he achieved his M.S. thesis at Harvard's Microrobotics Laboratory, where he is pursing research. His current research interests include flying robotics, soft sensors, and technology transfer.

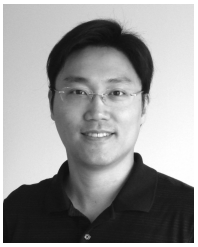

Yong-Lae Park received the M.S. and Ph.D. degrees in mechanical engineering from Stanford University, Stanford, CA, USA, in 2005 and 2010, respectively. He is currently a Technology Development Fellow with Wyss Institute, Harvard University. His current research interests include fiber optic force and tactile sensing, design of soft wearable robots for human rehabilitation and artificial skin with embedded soft sensors and actuators, and development of novel manufacturing processes for micro-robots and 3-D smart-robot-structures.

Robert J. Wood received the master's and Ph.D. degrees from the Department of Electrical Engineering and Computer Sciences, University of California, Berkeley, CA, USA, in 2001 and 2004, respectively. He is currently the Charles River Professor of Engineering and Applied Sciences in the School of Engineering and Applied Sciences and the Wyss Institute for Biologically Inspired Engineering, Harvard University. His current research interests include microrobotics and bioinspired robotics.